The Resonant Structure of xGEO and Implications for Cislunar Domain Awareness

Aaron J. Rosengren
University of California San Diego, La Jolla, CA, United States

Shane D. Ross
Virginia Tech, Blacksburg, VA, United States

Bhanu Kumar
Institute for Mathematics Universität Heidelberg, Germany

Anjali Rawat
Virginia Tech, Blacksburg, VA, United States

ABSTRACT

A rigorous dynamical definition for beyond GEO (xGEO) is the critical distance at which the secular contributions from the lunisolar perturbations exceed those from Earth oblateness, known in astronomical parlance as the Laplace radius. xGEO fundamentally represents a restricted four-body problem (R4BP), which can be approached locally using the perturbed-Hamiltonian formulation or globally using techniques stemming from the R3BP. Remote sensing, regardless of the phenomenology, must accommodate the complex dynamics in this domain. A many-sided and detailed investigation of the resonant structure of xGEO space, aside from its own particular significance, is of prime importance for space domain awareness as such resonances significantly affect the global structure of orbital phase space. In contrast to the traditional LEO-to-GEO domain, the predominant resonances in xGEO are governed by octupolar perturbations to the classical von Zeipel-Lidov–Kozai dynamics, among, hitherto, unstudied interactions with the lunar orbital and precession frequencies. This paper combines the local picture provided by the perturbed-Hamiltonian formulation of xGEO astrodynamics with the global geometric dynamical portrait provided by semi-analytical, dynamical-systems theory approaches to the restricted three-body problem, harnessing these in unique ways to probe for the first time the high time-resolution details of the strongly chaotic orbital evolution of distant cislunar space probes. This research uncovers the phase-space structure and connectivity of xGEO, identifying both highly stable 'graveyard' orbits, as well as chaotic-trajectory regimes that can most easily mask maneuvers. Results yield improvements over current capabilities by discovering and exploiting the multiscale spatio-temporal, dynamical structure of cislunar phase space from very distant, highly eccentric, Earth-bound satellites to lunar mean-motion resonances and their invariant manifolds.

1. INTRODUCTION

As new transportation, communication, and logistic infrastructures are being planned and developed for cislunar space in the Earth-Moon system, the need for improved space domain awareness (SDA) beyond the geostationary belt (xGEO) becomes paramount [1– Cislunar space refers to the orbital regimes about the Earth out to and including the region around the surface of the Moon. A wide variety of dynamical models are employed to approximate the vast diversity of cislunar trajectories. Whereas circumterrestrial and circumlunar orbits are largely governed by the perturbed two-body problem (P2BP) [4], in which the effects of the non-spherical gravity field and third-body perturbations on Earth or Moon satellites are often treated in a perturbed-Hamiltonian formulation (see, e.g., [5–7 all other cislunar trajectories—including lunar transfers, libration-point orbits (LPOs), Earth-Moon cyclers, stable and unstable mean-motion resonances (MMRs), and a wealth of other exotic periodic and non-periodic orbits—are specific applications of the gravitational N-body problem [8–1 The mathematical model adopted in the latter case is the restricted

three-body problem (R3BP), in which the spacecraft of negligible mass is simultaneously affected by the terrestrial and lunar gravitational forces. This framework efficiently captures Earth-Moon orbital transfers [8, 9], models the regions of the Lagrange equilibrium points (with L_1 and L_2, demarcating the lunar Hill sphere, approximately located at 51 and 69 Earth radii, respectively, in Figure 1), and has generally been the most studied formulation of motion in cislunar space. Developing and maintaining a space object catalog (SOC) for cislunar space beyond GEO, however, will require significant improvements in our understanding of the way objects behave in this complicated multi-body environment over orbital, decadal, and even centennial timescales. Most studies to date have only focused on the orbital timescales of LPOs within the framework of the circular, restricted, three-body problem (CR3BP) [15–17] or a hierarchy of more realistic, and more complicated, dynamical models [18–21]. Of the myriad of trajectories uncovered by these fundamental mathematical models, the distant retrograde orbits [22–24] and near-rectilinear halo orbits [18, 25–28] have assumed a special significance. There is, however, a dynamical plethora of Earth-bound trajectories in xGEO space that must be more deeply understood to enable robust cislunar SDA [29, 30]; see, e.g., Figure 1, which highlights the orbital-element distributions of cataloged xGEO space objects.

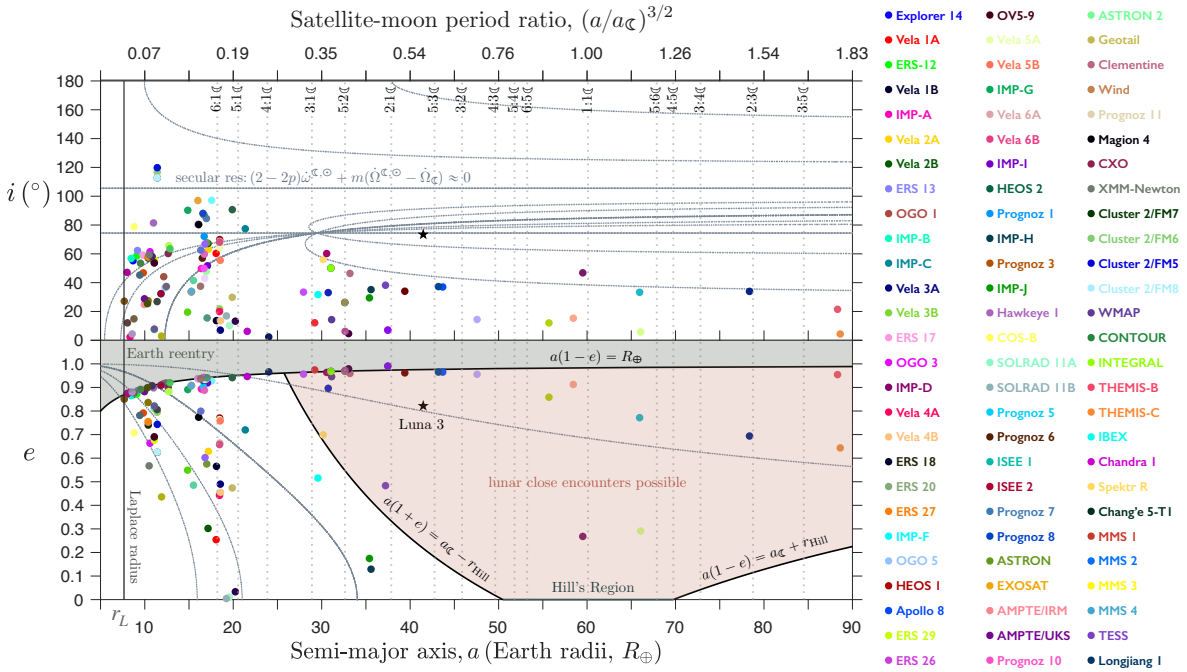

Fig. 1: A snapshot of the historic and current cataloged xGEO space objects in the planes of semimajor axis-ecliptic inclination (a, i) (*top panel*) and semimajor axis-eccentricity (a, e) (*bottom panel*), where the *colored circles* correspond to the osculating elements obtained from their latest TLE. The geocentric semi-major axis that distinguishes xGEO from a dynamical perspective—the Laplace radius (r_L)—is indicated by the *vertical line* at $a{\sim}7.7R_\oplus$ (q.v., Eq. 13 and Fig. 2). The approximate location of most principal lunar mean-motion (*vertical dashed lines*; Eq. 18) and secular resonances (other *curves*; Eq. 10) are shown. Objects located between the delimiting periapsis and apoapsis *curves* may enter the Moon's Hill sphere (Eq. 21), inducing discontinuous jumps in orbital elements á la Tisserand's criterion (Eq. 22). Luna 3, highlighted by the ⋆, is discussed further in [30]. Objects that reach the Earth-grazing $a(1-e) = R_\oplus$ *curve* may reenter the atmosphere. (`www.space-track.org`. Assessed 10 Mar. 2023)

For the investigation of the Earth's magnetosphere and the interplanetary space outside of it, satellites with orbits of high eccentricity, large inclination, and multi-day period are often used [**31**– Under the influence of the Moon and the Sun, a highly eccentric orbit of a deep-space probe can become nearly circular or a nearly circular orbit might become eccentric, while orbital inclination may also exhibit large shifts [**37**– NASA's eccentric Orbiting Geophysical Observatory (1964-054A), colloquially referred to as EGO, with an initial semi-major axis of 12.7 Earth radii and an eccentricity of 0.918, is particularly interesting as it only reentered in August 2020 (see Figure 10, discussed in §4), in contrast to earlier predictions that indicated

a lifetime of only 16 years [37]. A more modern example is ESA's International Gamma-Ray Astrophysics Laboratory (INTEGRAL) satellite (72-hour period with $e \sim 0.9$), which despite the longevity of its original operational orbit (orbital lifetime greater than two centuries), will now come down in 2029 as its orbit was modified via a series of four thruster burns [45].

For orbits where the semi-major axis is a substantial fraction of the Moon's, several orbital revolutions may be sufficient to lower the perigee height below the Earth if an unfavorable orbital configuration is chosen [46–48]. Among the first and perhaps the most interesting of this class of very distant, highly eccentric satellites was the Soviet space probe, Luna 3 (1959 Theta 1), which circumnavigated the Moon (passing through its sphere of influence) and returned to the Earth on a new elliptical trajectory. Luna 3 twice suffered close approaches with the Moon, and despite having an initial perigee height outside of the GEO belt, after only 11 revolutions, its eccentricity increased to the point that it became an Earth-crosser, plummeting back into the atmosphere [30, 49]. The lunar flybys and subsequent orbital motion of Luna 3, and its dramatic crash, are extremely interesting from the standpoint of astrodynamics; a satisfactory treatment of the problem, however, was only given recently in [30].

The Interstellar Boundary Explorer (IBEX) and the Transiting Exoplanet Survey Satellite (TESS), two modern Luna-3 like orbits, are distinguished by their high apogee distances and lunar MMR phasing [36, 50]. IBEX (2008-051A), with its nominal mission lasting only two years, had to change its operational orbit for its extended mission to avoid violating altitude and eclipse mission constraints. Its nominal orbit turned out to be chaotic and unpredictable beyond 2.5 years, as a result of significant, though hitherto uncharacterized, lunar perturbations, and IBEX was subsequently placed in a novel 3:1 MMR with the Moon ($P_M/3$). Following suit, TESS (2018-038A) orbits in a 2:1 lunar MMR ($P_M/2$), which was established using a lunar swing-by maneuver. Though not explicitly stated in its published orbit design [51], Russia's Spektr R (2011-037A) also seemingly orbits in or near the lunar 3:1 MMR, but with a significantly high ecliptic inclination to further permit Kozai-Lidov oscillations [30, 52] and other secular-resonant phenomena.

Combining observations, theory, and simulation, this research casts light on the multiscale spatio-temporal dynamics of geocentric and selenocentric orbits (governed by the P2BP), libration-point and other exotic three-body orbits (governed by the R3BP) in a holistic fashion. This investigation combines the "global" geometric dynamical portrait provided by semi-analytical approaches to the 3BP with the "local" picture provided by more specialized P2BP methods focused on specific regions of phase space. The scope of work covers the wide range of orbital phase space relevant to both historic and current cislunar missions (see, e.g., Figure 1) launched by the U.S. (e.g., AMPTE, Chandra X-ray Observatory, several EXPLORER series satellites, ARTEMIS), Europe (e.g., XMM-Newton, Cluster II), Russia (e.g., Prognoz, Spektr-R, ASTRON), China (e.g., Chang'e, Longjiang), as well as the significant future xGEO missions scheduled or proposed by over a dozen nations or organizations to be launched in this decade.

2. PHASE-SPACE STRUCTURE AND CONNECTIVITY OF CISLUNAR XGEO SPACE

2.1 Perturbed-Hamiltonian Formulation

Many physical systems can be modeled as having an underlying dynamical skeleton that organizes and governs how all the possible behaviors are related. The global properties of multidimensional, nearly integrable Hamiltonian systems are determined by the relative location and size (widths) of the predominant resonances [53, 54]. The dynamical environment occupied by artificial celestial bodies is subject to motions that are widely separated in frequency: the earthly day, the lunar month, the solar year, and various precession frequencies originating from the gravitational action of the Sun on the Earth-Moon system. Primary among these is the regression of the Moon's line of nodes with a period of about 18.61 years, and a progression of the lunar apsidal line with a period of roughly 8.85 years. The provision of frequencies in the Earth–Moon–Sun system gives rise to a diverse range of complex resonant phenomena associated with orbital motions. Resonances affecting satellites in the traditional geocentric domains, from low-Earth orbit (LEO) to GEO, have had such thorough attention accorded to their study that the outstanding difficulties are thought to be solely in the final refinements [4]. The occurrence and nature of the secular resonances driving the long-term dynamics of medium-Earth orbits (MEOs), for instance, depend chiefly on the regression of the lunar line of nodes [5]. These secular resonances, involving linear combinations of the satellite's apsidal and nodal

precession rates ($\dot{\omega}$ and $\dot{\Omega}$, largely forced by Earth's oblateness) and the rate of lunar node motion ($\dot{\Omega}_{\leftmoon}$, on account of the Sun's gravitational action), occur in profusion so that the orbital phase space is densely threaded by an exceedingly complicated web-like structure.

2.1.1 A Review of the Secular Resonances in MEO

Mathematically, in action-angle variables (J, Φ), the 2.5 degrees-of-freedom (DOF), orbit-averaged Hamiltonian of the MEO problem loosely reads [qq.v., 5, 55]

$$\begin{aligned} \mathcal{H} &= \mathcal{H}_{\rm sec}(J) + \epsilon \mathcal{H}_{\rm lp}(J, \Phi), \quad \epsilon \ll 1 \\ &= \mathcal{H}^{\rm Kep} + \mathcal{H}^{\oplus} + \mathcal{H}^{\leftmoon} + \mathcal{H}^{\odot}, \end{aligned} \tag{1}$$

where $\mathcal{H}^{\rm Kep} = -\mu_{\oplus}^2/2L^2$ is the Kepler Hamiltonian ($L = \sqrt{\mu_{\oplus} a}$), which depends only on the mean semi-major axis, treated as a parameter in the averaged problem (i.e., the satellite's mean anomaly M is a cyclic variable and consequently a is constant on average), $\mathcal{H}^{\oplus}$ is the classical orbit-averaged Hamiltonian for the oblateness perturbation, and the lunar and solar perturbing Hamiltonians are developed as Fourier-Taylor series of complicated structure (Kaula-like expansions [55]), e.g.,

$$\mathcal{H}^{\leftmoon} = -\sum_{m=0}^{2} \sum_{p=0}^{2} \sum_{s=0}^{2} h^{\leftmoon}_{2-2p,m,\pm s} \cos \Phi^{\leftmoon}_{2-2p,m,\pm s}, \tag{2}$$

whose arguments are combinations of the orbital phase and orientation angles of the satellite (ω and Ω) and the perturbers (i.e., $\Phi(\omega, \Omega, \Omega_{\leftmoon})$), and whose coefficients depend on the size and shape (semi-major axes and eccentricities) of their orbits and the inclinations (i.e., $h(a, e, i, a_{\leftmoon}, e_{\leftmoon}, i_{\leftmoon})$).

The extended autonomous Hamiltonian (without the Keplerian part), expressed in the Delaunay ($G = L\sqrt{1-e^2}, H = G\cos i, g = \omega, h = \Omega$) and appended canonical variables (Γ, τ), such that $\dot{\tau} \equiv \partial \mathcal{H}/\partial \Gamma = \dot{\Omega}_{\leftmoon}$, has the form

$$\mathcal{H}(G, H, \Gamma, g, h, \tau; L) = \mathcal{H}_{\rm sec}(G, H; L) + \mathcal{H}_{\rm lp}(G, H, g, h, \tau; L) + \dot{\Omega}_{\leftmoon}\Gamma, \tag{3}$$

in which

$$\begin{aligned} \mathcal{H}_{\rm sec}(G, H; L) &= \mathcal{H}^{\oplus}_{\rm sec} + \mathcal{H}^{\leftmoon}_{\rm sec} + \mathcal{H}^{\odot}_{\rm sec}, \\ \mathcal{H}_{\rm lp}(G, H, g, h, \tau; L) &= \mathcal{H}^{\leftmoon}_{\rm lp} + \mathcal{H}^{\odot}_{\rm lp}. \end{aligned} \tag{4}$$

The secular perturbations due to Earth oblateness is described by

$$\mathcal{H}^{\oplus}_{\rm sec}(G, H; L) = \frac{J_2 R_{\oplus}^2 \mu_{\oplus}^4}{4L^3} \frac{G^2 - 3H^2}{G^5}, \tag{5}$$

where J_2 is the second, zonal-harmonic coefficient of the geopotential, $R_{\oplus}$ is the mean equatorial radius of the Earth, and $\mu_{\oplus}$ denotes the Earth's gravitational parameter. Secular perturbations due to the Moon and the Sun are related to terms in their expansions in Eq. (2) with $2 - 2p = 0$, $m = 0$, and $s = 0$:

$$\begin{aligned} \mathcal{H}^{\leftmoon}_{\rm sec}(G, H; L) &= \frac{\mu_{\leftmoon}(3\cos 2\varepsilon_{\oplus} + 1)(2 - 3\sin^2 i_{\leftmoon})}{128 \mu_{\oplus}^2 a_{\leftmoon}^3 (1 - e_{\leftmoon}^2)^{3/2}} L^4 \left(5 - 3\frac{G^2}{L^2}\right)\left(1 - 3\frac{H^2}{G^2}\right), \\ \mathcal{H}^{\odot}_{\rm sec}(G, H; L) &= \frac{\mu_{\odot}(2 - 3\sin^2 i_{\odot})}{32 \mu_{\oplus}^2 a_{\odot}^3 (1 - e_{\odot}^2)^{3/2}} L^4 \left(5 - 3\frac{G^2}{L^2}\right)\left(1 - 3\frac{H^2}{G^2}\right), \end{aligned} \tag{6}$$

where $\varepsilon_{\oplus}$ is Earth's obliquity, $i_{\leftmoon}$ is the Moon's ecliptic inclination, and $i_{\odot}$ is the Sun's equatorial inclination. The long-periodic lunisolar perturbations are connected with $\dot{\Phi}^{\leftmoon}_{2-2p,m,\pm s} \not\equiv 0$. A lunisolar secular resonance occurs when a specific linear combination of the secular precession frequencies of the harmonic angles appearing in Eq. (2) is zero. That is,

$$\dot{\Phi}^{\leftmoon,\odot}_{2-2p,m,\pm s} = (2-2p)\dot{\omega} + m\dot{\Omega} \pm s\dot{\Omega}_{\leftmoon} \approx 0. \tag{7}$$

The mixed-reference-frame formalism of Eq. (2) permits us to consider the Moon's ecliptic inclination $i_{\mathbb{C}}$ as roughly constant and the variation in $\Omega_{\mathbb{C}}$, largely caused by the disturbing action of the Sun, as approximately linear with a period of 18.61 years ($\dot{\Omega}_{\mathbb{C}} \approx -19.34\ ^\circ/\text{yr}$). It is quite fortuitous that under this (quadrupolar) order of series truncation, the secular, long-period, and resonant lunar and solar perturbations depend only upon the positions of their orbital planes and are not influenced by the positions of their perigees [38, 56–58]. Thus, the lunar apsidal progression ($\dot{\omega}_{\mathbb{C}} \approx 40.68\ ^\circ/\text{yr}$), can be ignored in the treatment of MEO dynamics.

The oblateness precession completely overshadows the lunisolar secular effects and other perturbing influences in MEO, as shown in Figure 2, so that ω and Ω have an essentially linear time dependence, with secular rates $\dot{g} = \partial\mathcal{H}^{\oplus}_{\text{sec}}/\partial G$ and $\dot{h} = \partial\mathcal{H}^{\oplus}_{\text{sec}}/\partial H$ with $\mathcal{H}^{\oplus}_{\text{sec}}$ in Eq. (5). In the Keplerian elements, the satellite orbital evolution is given by the classical expressions,

$$\dot{\omega} \approx \dot{\omega}^{\oplus} = \frac{\omega^{\oplus}}{2}\frac{5\cos^2 i - 1}{(1-e^2)^2}, \quad \dot{\Omega} \approx \dot{\Omega}^{\oplus} = -\omega^{\oplus}\frac{\cos i}{(1-e^2)^2}, \tag{8}$$

where

$$\omega^{\oplus} = \frac{3}{2}\sqrt{\mu_{\oplus}}J_2 R_{\oplus}^2 a^{-7/2}. \tag{9}$$

2.1.2 Lunisolar Secular Resonances Beyond GEO

Several important theoretical strides [4, 5, 55, 59] have been made in understanding various aspects of the secular chaos affecting the Earth's satellites in the complex resonance environments from LEO to GEO. Despite over sixty years of space activity, however, we know amazingly little about the multiscale dynamical environment beyond the traditional geocentric regimes [29, 30]. Neglect of the lunisolar perturbations on the secular frequencies of nodal and apsidal precession, for instance, sets an upper limit to the radius of orbit for which the preexisting theory is valid ($a \lesssim 5R_{\oplus}$). At geosynchronous altitude, however, the lunisolar perturbations are of the same order as the secular oblateness term [58, 60, 61], and must be included to accurately map out the resonance web; the outstanding difficulties of which have yet to be overcome [4]. Beyond the Laplace radius—the geocentric distance where the perturbing gravitational effects are equal ($\sim 7.7R_{\oplus}$; Figure 2), described below—the analysis must also be extended beyond quadrupolar gravitational interactions (i.e, Hill's approximation in the Legendre expansions in the ratio of semimajor axes) [56, 62, 63]. For the Sun, the effect of the third harmonic (parallactic, or octupole) term is negligible, while for the Moon, the contribution of the octupole ($l = 3$) term becomes more important as the orbital radius increases [4, 44]. Thus, for the xGEO regime, the lunisolar secular resonances are characterized by the general relation,

$$\dot{\Phi}^{\mathbb{C},\odot}_{l-2p,m,l-2q} = (l-2p)\dot{\omega} + m(\dot{\Omega} - \dot{\Omega}_{\mathbb{C}}) - (l-2q)\dot{\omega}_{\mathbb{C}} \approx 0, \tag{10}$$

where the secular apsidal and nodal rates are now dominated by lunisolar perturbations. The lunisolar precession can be obtained from Eq. (6) through the canonical relations $\dot{g} = \partial\mathcal{H}^{\mathbb{C},\odot}_{\text{sec}}/\partial G$ and $\dot{h} = \partial\mathcal{H}^{\mathbb{C},S}_{\text{sec}}/\partial H$:

$$\dot{\omega} \approx \dot{\omega}^{\mathbb{C},\odot} = \frac{\omega^{\mathbb{C}} + \omega^{\odot}}{2}\left(\frac{5\cos^2 i - 1 + e^2}{\sqrt{1-e^2}}\right), \quad \dot{\Omega} \approx \dot{\Omega}^{\mathbb{C},\odot} = -(\omega^{\mathbb{C}} + \omega^{\odot})\frac{1 + 3e^2/2}{\sqrt{1-e^2}}\cos i, \tag{11}$$

where [58, 60, 64],

$$\omega^{\mathbb{C}} = \frac{3}{4}\frac{\mu_{\mathbb{C}}}{\sqrt{\mu}}\frac{1 - \sin^2 i_{\mathbb{C}}/2}{a_{\mathbb{C}}^3(1-e_{\mathbb{C}}^2)^{3/2}}a^{3/2}, \quad \omega^{\odot} = \frac{3}{4}\frac{\mu_{\odot}}{\sqrt{\mu}}\frac{1}{a_{\odot}^3(1-e_{\odot}^2)^{3/2}}a^{3/2}; \tag{12}$$

Here, the orbital elements of the satellite, lunar, and solar orbits are all relative to the ecliptic.

The above analysis leads us naturally to a rigorous dynamical definition for xGEO as the critical distance at which the secular contributions from the lunisolar perturbations exceed those from Earth oblateness. This is known in astronomical parlance as the *Laplace radius* r_L [65] and is defined in the Earth-Moon-Sun context by [64],

$$r_L^5 = a^5\frac{\omega^{\oplus}}{\omega^{\mathbb{C}} + \omega^{\odot}} = 2\mu_{\oplus}J_2R_{\oplus}^2 \Big/ \left(\frac{\mu_{\mathbb{C}}}{a_{\mathbb{C}}^3}\frac{1 - \sin^2 i_{\mathbb{C}}/2}{(1-e_{\mathbb{C}}^2)^{3/2}} + \frac{\mu_{\odot}}{a_{\odot}^3}\frac{1}{(1-e_{\odot}^2)^{3/2}}\right) \approx 7.7R_{\oplus}. \tag{13}$$

Figure 2 shows a graphical depiction of the Laplace radius and thus, our new dynamical definition of xGEO. Beyond r_L, the effects of atmospheric drag are negligible, even for near Earth-grazers [37, 38, 41, 42, 66], and solar radiation pressure (SRP) secular perturbations [qq.v., 64, 67] are several orders of magnitude smaller than lunisolar, even for high area-to-mass ratio objects ($A/m > 1$ m^2/kg). Therefore, xGEO fundamentally represents a restricted four-body problem (R4BP), which can be approached locally using the perturbed Hamiltonian formulation outlined herein or globally using techniques stemming from the R3BP.

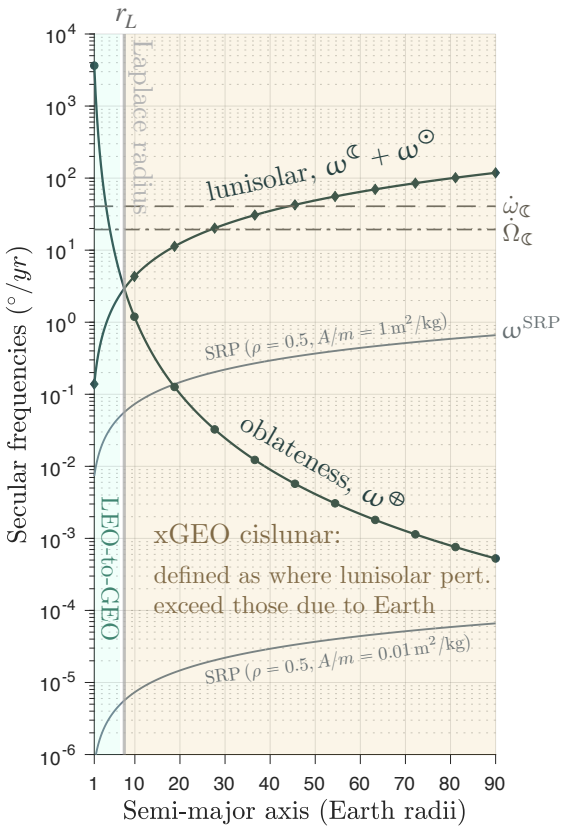

Fig. 2: Our proposed definition for xGEO based on the *Laplace radius*, r_L, beyond which the secular frequencies of nodal and apsidal precession from lunisolar perturbations (Eq. 11) exceed those of Earth oblateness (Eq. 8). The approximately constant rates of lunar apsidal progression ($\dot{\omega}_{\leftmoon} \approx 40.68\ ^\circ$/yr) and nodal precession ($\dot{\Omega}_{\leftmoon} \approx -19.34\ ^\circ$/yr) are also shown, together with the secular rates of solar radiation pressure (SRP) for both a low and high area-to-mass (A/m) ratio object of reflectivity ρ [qq.v., 64, 67].

2.1.3 The Kozai-Lidov Secular Resonance

Until the advent of artificial satellites of the Earth (1957) and the Moon (1966), astronomical applications of the problem of three bodies was largely limited by the principal traffic rules obeyed by most celestial bodies of the Solar System. This conditioned their heliocentric orbits to be nearly coplanar and characterized by only moderate eccentricities; accordingly, an expansion of planetary perturbations in ascending powers of their orbital eccentricities or the inclination of their orbits to the invariable plane of the Solar System constituted the usual avenue of approach [68]. The outstanding exception was the asteroids and comets [69], many of their orbits were observed to be highly eccentric and inclined, with their motions, upon decades of scrutiny, found to be subjected to a multitude of orbital resonances. With the launch of the Space Age, similar dynamical situations, every bit as varied and rich as those in the asteroid belt, can occur in closer proximity to our terrestrial abode [57].

The dynamical system given by Eq. (1), for large planetocentric distances where the quadrupolar moment from the equatorial bulge of Earth can be ignored, and under the approximation that the Moon's orbital plane coincides with the ecliptic, is mathematically equivalent to the system originally treated by Lidov [57, 62] and Kozai [69], who discovered a phenomenon of the most far-reaching significance [52, 70]. The CR4BP (doubly-averaged) Hamiltonian (without the Keplerian part) takes the form

$$\mathcal{H}_{\text{vZLK}} = -\frac{a^2}{8}\left(\frac{\mu_\odot}{a_\odot^3} + \frac{\mu_{\leftmoon}}{a_{\leftmoon}^3}\right)\left[2 + 3e^2 - 3\left(1 - e^2 + 5e^2\sin^2\omega\right)\sin^2 i\right], \tag{14}$$

where all angular elements are with respect to the ecliptic plane. This autonomous Hamiltonian system is integrable and possesses three integrals, $c_0 = a = \text{constant}$ (due to orbit averaging), and

$$c_1 = \left(1 - e^2\right)\cos^2 i = \text{constant}, \tag{15}$$

$$c_2 = e^2\left(\frac{2}{5} - \sin^2 i \sin^2\omega\right) = \text{constant}. \tag{16}$$

Substituting the value of $\sin^2 i$ from Eq. (15) into Eq. (16) results in an alternate expression for c_2 as a function of (c_1, e, ω),

$$c_2\left(e, c_1, \omega\right) = e^2\left[\frac{2}{5} - \left(1 - \frac{c_1}{1 - e^2}\right)\sin^2\omega\right]. \tag{17}$$

Solutions can be visualized in the $(\omega, X \triangleq \sqrt{1-e^2})$ plane as isolines of the c_2 integral, for a given c_1. These flow plots, as originally presented by [62] and [69], are called von Zeipel–Lidov–Kozai diagrams [70].

There exist stationary solutions ($\omega = \pi/2$ and $\omega = 3\pi/2$) such that $\dot{\omega} = 0$ above a critical inclination $i_{\text{crit}} \approx 39.2^\circ$. Close to these fixed points, the argument of perigee librates on secular timescales exciting coupled oscillations (Kozai-Lidov (KL) cycles) in eccentricity and inclination, according to Eq. (15). Qualitatively different behaviors can occur when the octupole moment of the Legendre expansion is accounted for in the secular dynamics [52]; orbits can reach extremely high eccentricities and undergo chaotic flips from prograde to retrograde orientation. We thus expect that xGEO objects with ecliptic inclinations greater than 39.2° (see, e.g., Figure 1) will be affected by octupolar perturbations to the KL dynamics (i.e., the eccentric KL resonance), among other yet unstudied interactions with the lunar orbital and precession frequencies; e.g., nonlinear secular (Eq. 10) and mean-motion resonances (Eq. 18).

2.1.4 Lunar Mean-Motion Resonances.

While mean-motion resonances (commensurabilities of orbital periods) constitute one of the most important and far-reaching aspects of dynamical astronomy [68], they have remained woefully underrated in Earth-satellite dynamics in part because the orbits of most satellites thus far are too low to be affected by mean-motion commensurabilities. "What are the Kirkwood gaps of cislunar space?" is a question of great current interest for mission planners as we are locating our space-based assets, such as the IBEX and TESS [36, 50], in predominant lunar MMRs that have hitherto only been treated in piecemeal. Also of special note is ESA's SMART-1 low-thrust spiraling trajectory to the Moon, which used a combination of multiple coast arcs and weak lunar gravity assists on account of passage through lunar MMRs [71]. The effects of these resonances were to raise the perigee and to rotate the orbit both in inclination and argument of perigee, enabling the subsequent lunar capture [15].

Standard tools have been developed to calculate the width (strength) and location of mean-motion resonances [72, 73]. A satellite with mean motion $n = \sqrt{\mu_\oplus/a^3}$ is in resonance with the Moon with mean motion $n_{\leftmoon} = \sqrt{\mu_\oplus/a_{\leftmoon}^3}$ when,

$$\begin{aligned}\dot{\Phi}_{lmphqj} &= (l-2p+q)\dot{M} - (l-2h+j)\dot{M}_{\leftmoon} + (l-2p)\dot{\omega} - (l-2h)\dot{\omega}_{\leftmoon} + m(\dot{\Omega} - \dot{\Omega}_{\leftmoon}) \approx 0 \\ &\approx (l-2p+q)n - (l-2h+j)n_{\leftmoon} = 0,\end{aligned} \tag{18}$$

as the secular frequencies are generally much smaller than the orbital frequencies $(l, m, p, h, q, j \in \mathbb{Z})$. A $k{:}k_{\leftmoon}$ lunar MMR thus occurs when the satellite's semi-major axis, assuming unperturbed Keplerian motion,

satisfies $a \approx a_{k:k_{\mathbb{C}}}$ where,

$$a_{k:k_{\mathbb{C}}} = \left(\frac{k}{k_{\mathbb{C}}}\right)^{2/3} a_{\mathbb{C}}. \tag{19}$$

The resonant motion imposes librations of Φ around an equilibrium value, correlated to oscillations of the semi-major axis a, though its value remains between limits (chaotic resonance zones) defined by the borders (or separatrices) of the unstable periodic resonances. The approximate centers of many principal (low-order) lunar MMRs are shown in Figure 1 in §1. While the perturbed-Hamiltonian formulation can permit the calculation of the resonant half-width excursions in (a, e, i) and a local characterization of the resonances, the MMR problem is more amenable to semi-analytical and numerical techniques relying fundamentally on the R3BP framework.

3. RESTRICTED MULTI-BODY DYNAMICAL-SYSTEMS THEORY

The simplest model that approximates the motion of real objects in cislunar space, the circular, restricted three-body problem (CR3BP), has orbital solutions that display a surprising degree of complex transport phenomena. This idealized mathematical model consists of a massless satellite, and two massive bodies (e.g., Earth and Moon) moving in circular orbits about their common center of mass; see Figure 3 (*left*).

The CR3BP dynamics for the satellite, much like the perturbed two-body approaches shown above, can be formulated as a Hamiltonian with,

$$\mathcal{H}_{\text{CR3BP}} = \tfrac{1}{2}((p_x + y)^2 + (p_y - x)^2 + p_z^2) + \bar{U}, \tag{20}$$

where, in standard re-scaled coordinates, p_x, p_y, and p_z are the momenta conjugate to the rotating frame x, y, and z coordinates, respectively, and $\bar{U}$ is the effective potential in Figure 3.

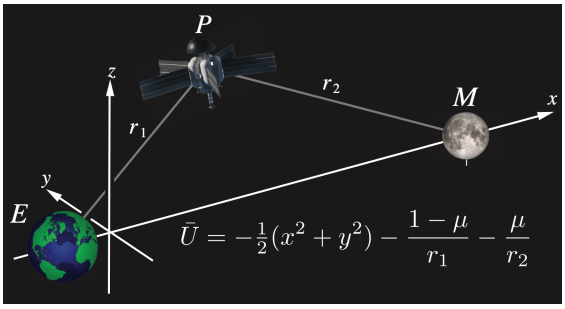

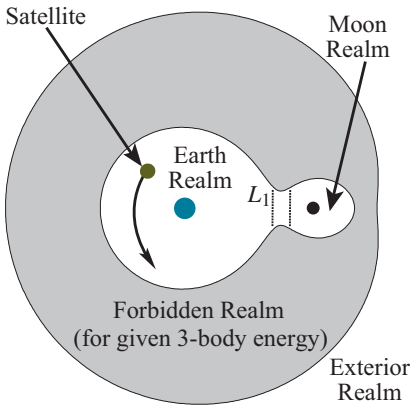

Fig. 3: A satellite P, in the field of the Earth and Moon, in the xyz rotating frame, whose dynamics are governed by the re-scaled effective potential $\bar{U}$ (with mass parameter $\mu = \mu_{\mathbb{C}}/(\mu_{\oplus} + \mu_{\mathbb{C}}) = 0.01215$) and a Coriolis force (*left*). The connectivity of the three realms of phase (*right*) is given by the three-body energy, Eq. (20); this is between the energies of L_1 and L_2. The region bounding the Moon realm is the Hill sphere (Eq. 21).

The Earth-Moon Lagrange points are the five stationary solutions or equilibria in the *rotating frame*, co-orbiting with the Earth and Moon, where L_1, L_2, and L_3 lie along the Earth-Moon line, and L_4 and L_5 form equilateral triangles with them. The Moon's Hill region is a sphere between the points L_1 and L_2, in which the motion of the satellite is dominated by the attraction of the Moon. A lunar encounter is defined as $r_2 < r_{\text{Hill}}$, approaching within one Hill radius,

$$r_{\text{Hill}} \approx a_{\mathbb{C}} \left(\tfrac{\mu}{3}\right)^{1/3} \simeq 9.6 R_{\oplus}; \tag{21}$$

thus, a significant portion of xGEO orbital space is capable of experiencing a close encounter (Figure 1).

The Lagrange points are in a sense the "seeds" that give rise to several continuous and interlocking families of periodic orbits in the rotating frame, as shown in the stylized bifurcation diagram of Doedel et al. [11]. Note that many of these orbits spend much of their time far away from any Lagrange point, and some even span much of xGEO space.

Associated with the collinear unstable Lagrange points (a.k.a., libration points), or their dynamical extensions to periodic or quasi-periodic orbits [19], are stable and unstable manifolds, phase-space structures that asymptotically approach or depart the Lagrange points (or their dynamical extensions). The libration-point orbits (LPOs) most often treated in the literature— the Lyapunov and halo orbits—reside in the bottlenecks in the three-body energy surfaces that partition the entire phase space into three main orbital realms [14]: Earth realm, Moon realm, and exterior realm; see Figure 3 (*right*).

Taking a holistic phase-space point of view, the cislunar region beyond GEO is composed of intermingled chaotic and quasi-periodic regions, as illustrated in Figure 4. Solutions of the R3BP form the global template of motion in xGEO. That is, solutions of the R3BP are to the xGEO formulation as Kepler's solutions to the 2BP are to traditional near-Earth perturbation theory. In fact, for local dynamics in the R3BP, methods from the perturbed 2BP, mentioned above, are useful. Unlike the 2BP, however, which has many mathematical symmetries leading to many constants of motion and closed-form geometric and analytical descriptions of the motion in terms of the conical orbital elements, the 3BP possesses only one constant of motion—the Jacobi integral, a re-scaled version of the Hamiltonian function, $C_J = -2\,\mathcal{H}_{\mathrm{CR3BP}}$. An approximation to the Jacobi constant in orbital-element space with respect to the Moon is the Tisserand parameter ($T_{\mathfrak{C}} \approx C_J$), defined as

$$T_{\mathfrak{C}} = \frac{a_{\mathfrak{C}}}{a} + 2\cos i\sqrt{\frac{a}{a_{\mathfrak{C}}}(1-e^2)}, \tag{22}$$

which plays a role in dynamically limiting the range of chaotic motion a satellite is capable of, without a maneuver, in the orbital elements (a, e, i), as in Figure 5.

Cislunar SDA in xGEO captures not only an unprecedented 2000+ volumetric expansion over GEO [3], but also a dramatic change in the fundamental motion of space objects, as explicated herein. The nonlinear astrodynamics in xGEO, encompassing secular, resonant, chaotic, close-encounter, and manifold dynamics, is dramatically different than the weakly perturbed two-body approach used for over a half century for the detection and tracking of objects near Earth. Yet, to date, only the relatively short timescale dynamics of LPOs and their associated invariant manifolds have been partially coupled with the cardinal questions and problems posed by cislunar SDA. Lunar MMRs also significantly shape cislunar dynamics forming stable-unstable pairs, with corresponding intermingled chaotic and regular regions. The region of influence of the unstable resonant orbits (also called the chaotic resonance zone) can be rigorously defined using the separatrix of unstable resonant periodic orbits surrounding stable quasi-periodic regions (forming the stable resonance width), as detailed in [74]. Furthermore, the manifolds emanating from unstable MMRs can enable rapid dynamical transfers between resonances through heteroclinic connections [10].

4. RESULTS & EXPECTED IMPACTS

4.1 Uncovering the Resonant Structures of xGEO

Despite the preexisting theory on the cislunar regime, the unequivocal consensus of the astrodynamics community is that the motion of a satellite in this environment is highly chaotic, subject to rapid developments and unexpected changes in its orbital trajectory. These challenges are intensified when one considers the multiplicative complexity of remotely tracking multiple uncooperative space objects, each capable of frequent and unexpected changes in their orbital patterns through maneuvers and other events. Moreover, unlike the traditional geocentric orbits from LEO to GEO, where a satellite's nearly periodic orbit varies from sixteen to one rev/day, allowing for reliable updating of orbit estimates, the orbit periods for distant cislunar satellites are measured in days or weeks. Thus, tracking opportunities will be proportionally less, so the frequency and diversity of measurements needed for catalog updates will occur on longer timescales and with the propagation of orbits spanning longer time intervals between state updates. This becomes a critical issue as space objects enter periodic and pseudo-periodic orbits near the Earth-Moon Lagrange

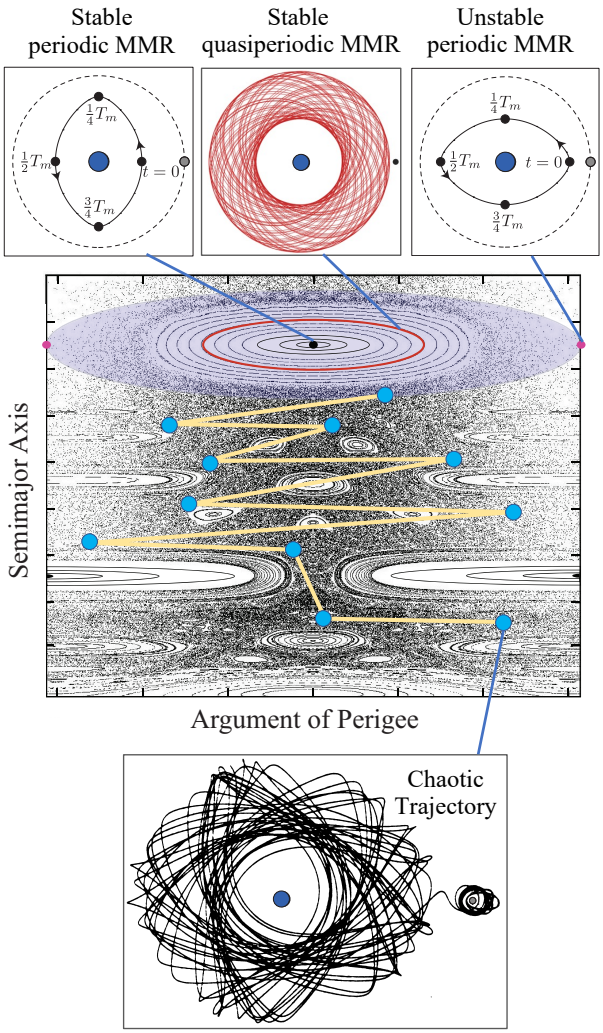

Fig. 4: Using action-angle variables, we obtain a global Poincaré section of stable resonance islands (*horizontal bands* of families of closed curves, representing slices of KAM tori) and the chaotic sea (*scattershot region*) going between them. Here, each point represents a trajectory. A resonant region, with various trajectories, is highlighted. The chaotic trajectory, starting in this resonant region, traverses widely through cislunar space, without any maneuvers. Note: all trajectories are shown in the rotating frame, and the *connecting lines* for the chaotic trajectory are just to guide the eye.

---

points, or into MMRs or other seemingly elusive three-body phenomena, where gravitational attractions traditionally considered perturbations can become dominant. Orbits in the Earth-Moon-Sun system beyond the Laplace radius (Eq. 13) are most accurately described by the restricted four-body problem, with the perturbed 2BP governing the local dynamics and the R3BP approaches governing global motions. Remote sensing, regardless of the phenomenology, must accommodate the complex dynamics in this domain.

Merging the global geometric dynamical portrait provided by semi-analytical approaches to the 3BP with the local picture furnished by more specialized perturbed 2BP methods will yield a much-needed integration of the fragmented knowledge regarding the complex dynamics of cislunar space. This holistic approach is demonstrated in Figure 5, underscroing the implications for understanding the multiscale astrodynamical environment beyond the traditional geocentric regimes. Many cataloged xGEO objects exhibit strong Kozai-Lidov effects, depicted as the backbone of the phase space (*top panel*), with their motions modulated by hitherto uncharacterized lunisolar perturbations to the underlying dynamical skeleton. There is no evidence

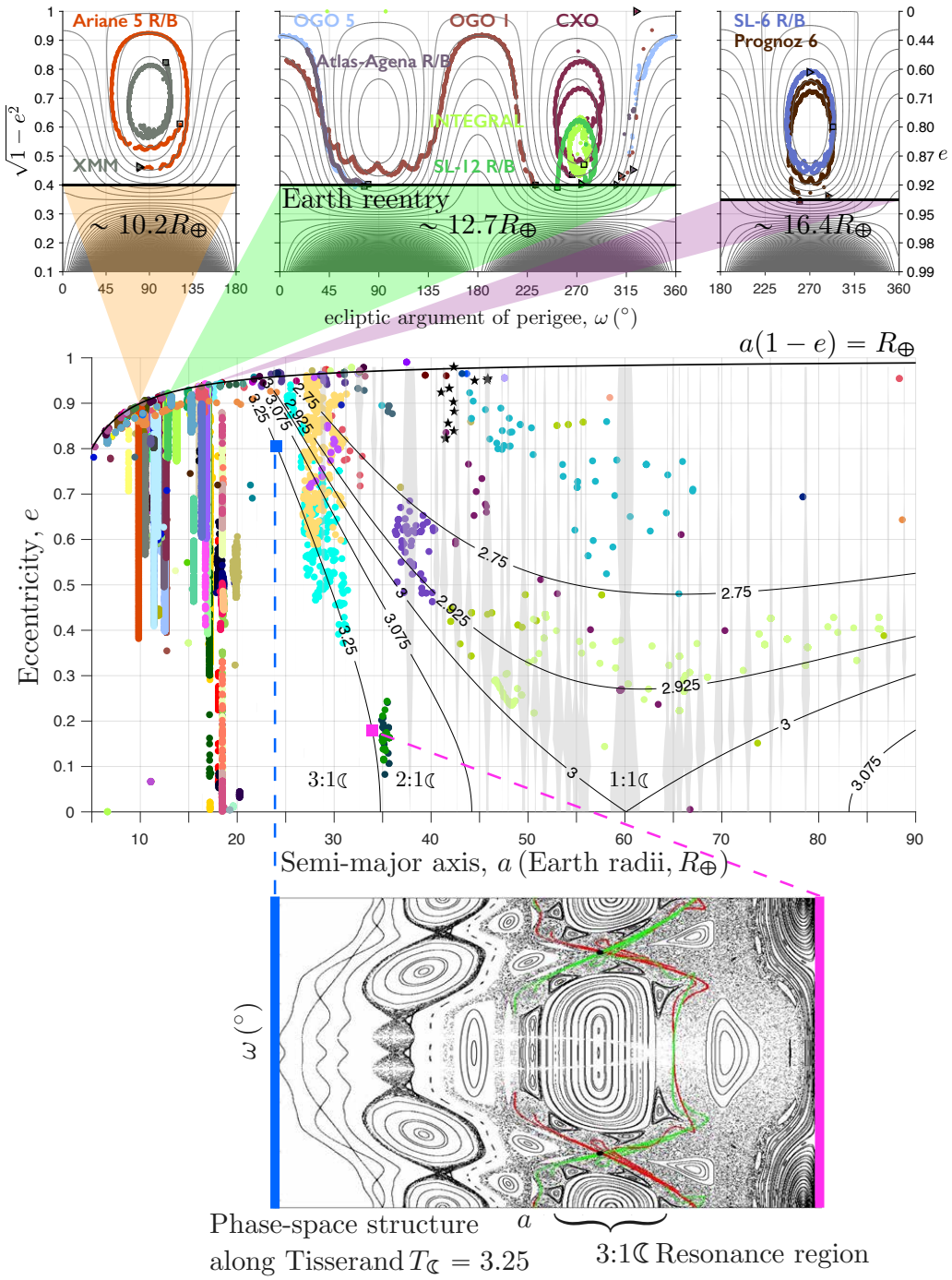

Fig. 5: The historic and current cataloged xGEO space objects in the semimajor axis-eccentricity ($a - e$) space (*middle panel*), superimposed on the atlas of MMRs, where each color corresponds to the two-line element (TLE) time histories of individual objects. The contours of constant Tisserand parameter, shown in *black*, and the widths of the predominant MMRs (*gray*) are both computed assuming that the objects and Moon are coplanar. The *top panel* shows a local analysis, from the perturbed Hamiltonian formulation, of the lunisolar Kozai-Lidov secular resonance (Eq 14) for the specific mean (orbit-averaged) semi-major axes, with the ephemerides of several actual xGEO objects overlaid (▷ indicates initial TLE and ▫ final). The *bottom panel* represents a global analysis, based on the R3BP dynamical-systems formalism, of the predominant lunar 3:1 MMR region. (www.space-track.org. Assessed 10 Mar. 2023).

of a secular change in the average value of their semi-major axes, hinting that their orbits are primarily governed by purely secular perturbations [68], which induce a variation in eccentricity, causing it to oscillate through a maximum value given by $e^2 \approx 1 - 5/3 \cos^2 i_0$, depending on its ecliptic initial inclination, provided that $|\cos i_0| \leqslant \sqrt{3/5}$ [52, 70]. The *middle panel* also displays, through crude approximations, an atlas of lunar MMRs in pseudo-action (a, e) space [72], indicating strong dynamical interactions among these orbital commensurabilities and giving rise to chaotic transport (*bottom panel*). The ephemerides of many cataloged objects in the Moon-crossing regions (see Figure 1) somewhat follow the contours of Earth-Moon-satellite three-body energy (Tisserand curves), which are superimposed on the *middle panel*, demonstrating significant unmodeled solar perturbations (i.e., the motion is fundamentally governed by the Earth-satellite-Moon-Sun R4BP). A more accurate representation of the global phase space of lunar MMRs is evinced for the 3:1 commensurability (*bottom panel*), where IBEX (2008-051A) and Spektr-R (2011-037A) are currently located.

The planar circular restricted three-body problem (PCR3BP), utilizing Poincaré map, can be employed to identify and map stable resonance widths and chaotic resonance zones onto the (a,e) plane [74] as shown in Figure 6. These widths effectively encompass the trajectories of various spacecraft, including IBEX, TESS, and Spektr-R, in contrast to the narrower semi-analytical resonance-width approximations traditionally used as shown in Figure 5 (*middle panel*). Importantly, the PCR3BP proves capable of accurately capturing the dynamics of even non-coplanar spacecrafts highlighting its utility in offering fundamental insights into spacecraft dynamics in cislunar space.

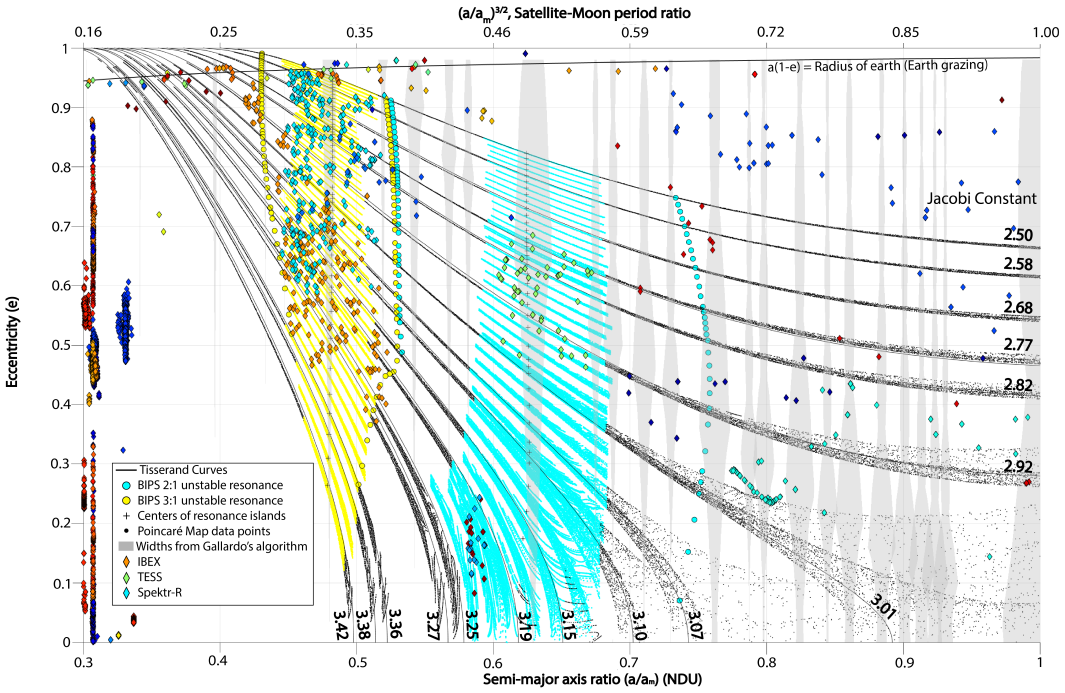

Fig. 6: TLEs of xGEO space objects are superimposed on PCR3BP widths which show larger stable resonance widths and delienates the region of influence of unstable periodic resonant orbits. The CR3BP resonance widths correctly capture the spread of space assets in the 2:1 and 3:1 stable resonance zones, namely IBEX, TESS, and Spektr-R

4.2 xGEO Orbit Parameterization and Predictions

The Joint Space Operations Center (JSpOC) maintains an up-to-date SOC of all trackable Earth-orbiting objects, made publicly available in the form of two-line element (TLE) sets. Though widely used for decades, there remain misunderstandings of the TLE usage, its accuracy, and limitations, as well as the limitations of the simplified general perturbation theory used to produce them (`SGP4`) [75]. While no covariance information

is provided, the estimated TLE positional accuracy at epoch is several hundred meters up to several km (1-sigma) for LEO, a few km for MEO, up to tens of km for GEO, and dozens of km for highly eccentric orbits [76, 77]. The TLEs provide Brouwer-Lyddane mean element, which can be converted to osculating elements, and hence a state vector, by reconstituting the removed short-periodic terms with `SGP4`. A more accurate initial state and an estimation of the initial covariance and object properties can be obtained by considering a batch of historical TLEs, converted from mean to osculating elements, as pseudo-observations, and then applying a batch least-squares differential corrector to this TLE window, using a high-precision numerical propagator [78–81].

Accurate modelling and simulation capabilities, in concert with knowledge of relevant phase-space structures, can be adapted to processes that support the ground- and space-based surveillance and maintenance of xGEO to holistically improve cislunar SDA. Such investigations can enable observers to decide where and when data should be obtained in future campaigns, for example, by providing stringent constraints through stability analysis of the existing and predicted orbits. For full ephemeris numerical simulations, we leverage the state-of-the-art `IAS15` integrator in `REBOUND` [82] and `ASSIST` [83], adapting them to be highly parallelizable for the efficient propagation of both the state dynamics and variational system for ensemble propagations.

A 30-day propagation of the orbit of TESS is shown Figure 8 under both the restricted Earth-Moon-Sun-satellite and Earth-Moon-satellite ephemeris models in `REBOUND`. We note that for TESS, only the more realistic 4BP physical model was able to reproduce the JPL Horizons ephemerides, indicating the limitations of simplified phenomenological models (e.g., the CR3BP). A roughly two-year propagation of the orbit of TESS is shown Figure 8 using `ASSIST`, compared to accurate Horizons data as well as TLEs. Figure 9 shows decadal evolutions of Spektr-R, based solely on TLE data (as this object is not listed within JPL Horizons). Spektr-R's resonant transition is accurately captured; the underlying dynamical mechanism driving this interesting behavior has yet to be fully identified and understood quantitatively.

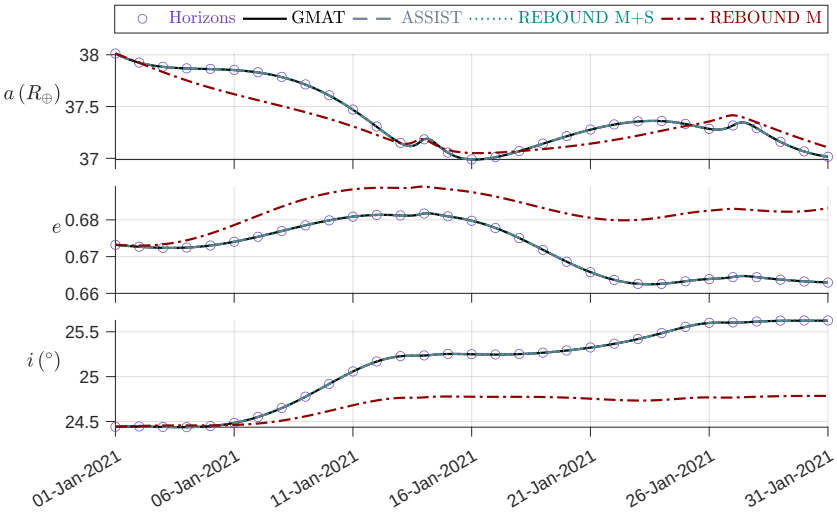

Fig. 7: Simulation of the evolution of TESS adapting a dynamical model in `REBOUND` [82, 84, 85] that contains both the Moon and Sun as perturbers (*cyan dotted curve*) or only the Moon (*red dashed-dotted curve*). Orbit propagations using `GMAT` [86, 87] (*solid gray curve*) and `ASSIST` [83] (*dashed gray curve*) are also shown for validation. The ephemeris obtain from the JPL Horizons web-service is overlaid as *purple circle*.

A basic question we are trying to solve is whether we can increase the predictive accuracy for cislunar objects, using only historical TLE data. There have been many interesting approaches to the TLE-based-prediction problem over the past decade, but the work of [78] deserves special mention here. They apply a batch least-squares differential correction to a TLE window, and fit an orbit to the state vectors derived from successive TLEs using a high-precision numerical propagator. By propagating the fitted orbit with the same high-fidelity code, they are able to obtain a 10-fold improvement over individual TLEs propagated with their associated analytic propagator (`SGP4`). We should note, however, that these propagations have

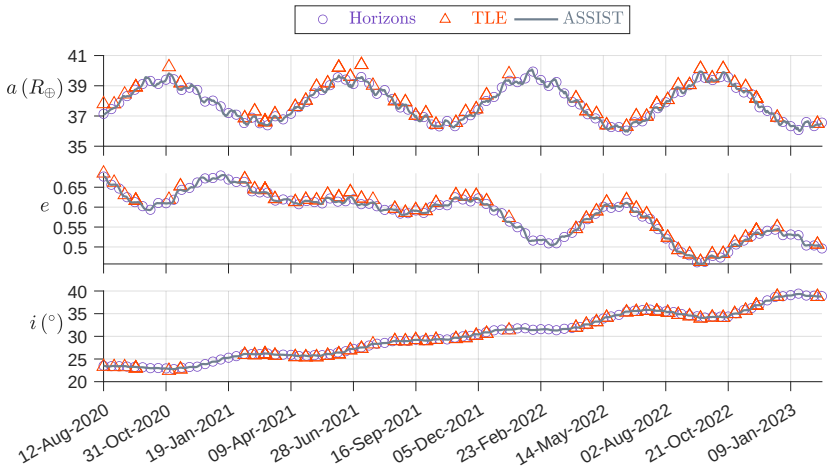

Fig. 8: Simulation of the orbital evolution of TESS using `ASSIST` [83]. The ephemeris obtain from the JPL Horizons web-service is overlaid as *purple circle* and TLEs as *orange triangles*.

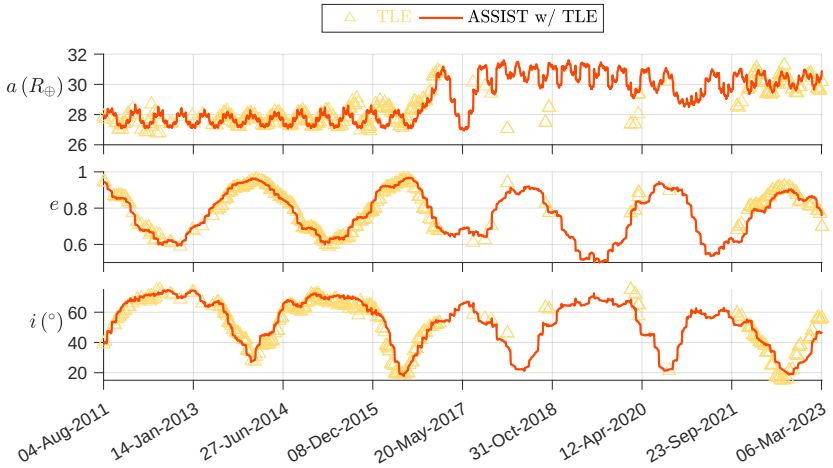

Fig. 9: Decadal simulations of the orbital evolution of Spektr-R using `ASSIST` [83]. The ephemeris obtain from the TLEs as overlaid as *triangles*.

been carried out over month timespans; accurate orbit predictions based on TLEs over decadal timespans is unprecedented, especially for distant xGEO space objects that are highly sensitive to initial conditions.

Figure 10 shows our recovery of the trajectory of OGO 1 (1964-054A), whose orbital lifetime was dramatically mis-predicted in the late 1960's [37]. Note the sparse observations during the operational lifetime of OGO, missing data points in the catalog for the next ∼30 years, and very dense TLEs starting in 2001 when tracking was resumed. Using our developed tools and methodologies, TLE data was utilized to successfully obtain more precise launch conditions of OGO, which, using `REBOUND`, we can completely recover its full multi-decadal trajectory and August 2020 decay using solely the initial state at orbit injection (i.e., without requiring further differential c orrection).[1] O rbit i mprovement b ased o n k nowledge o f t he O GO's secular and resonant motion, rather than orbit determination on the TLE pseudo-measurements [78– is used to

[1] Note that Earth oblateness has a negligible effect on the long-term evolution of the orbital parameters, but a very sharp short-periodic effect very near perigee, with the magnitude of the 'spike' depending on the height and position of p erigee. Accordingly, for our ephemeris modeling, we include all major sources of orbit perturbations, together with two-body regularization, to prevent the development of computational inaccuracies during the close-approach portion of the orbit.

obtain initial launch conditions that produced our ephemeris valid over the entire 56-year arc. The non-negligible collision risks posed by this LEO-to-GEO transiting spacecraft motivates both theoretical study and practical implementation.

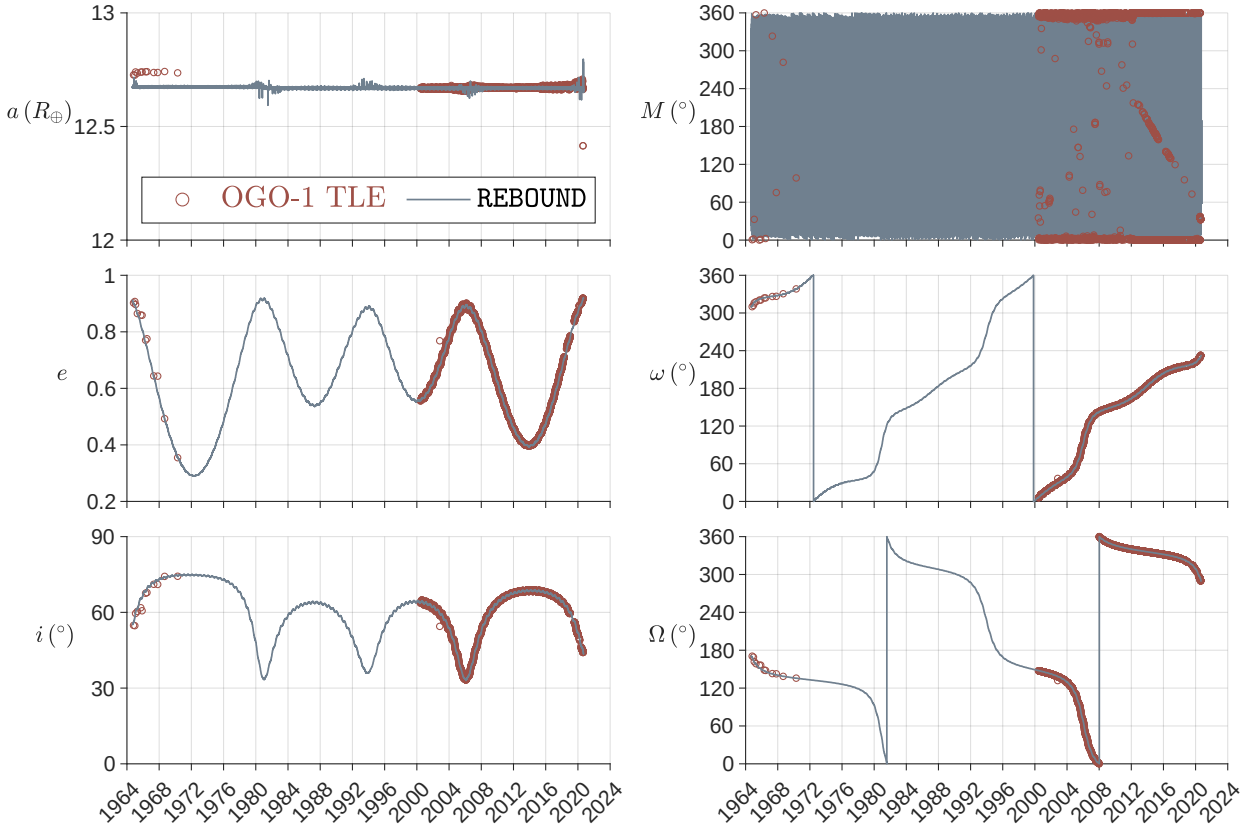

Fig. 10: The multi-decadal orbital evolution of NASA's Orbiting Geophysical Observatory (1964-054A) obtained using `REBOUND`, compared to TLEs. All angular elements are measured with respect to the ecliptic. This xGEO satellite was launched on 5 September 1964 into a very distant, elongated orbit, making tracking and prediction extremely challenging. Accordingly, 30 years of TLE data is missing from the public catalog. OGO 1 reentered 29 August 2020 in accordance with our prediction.

5. CONCLUSIONS AND OUTLOOK

Cislunar space, outside the confines of near-Earth satellite orbits, is poised to serve as a new high ground for space operations, and, like its circumterrestrial counterpart, must be sustained against risk from debris and other threats. It is precisely the distinctive and multi-faceted dynamical features of this regime that complicates SDA efforts and represents significant challenges for space sustainability. The insights and constraints from Hamiltonian mechanics can aid in detection and tracking amidst this new dynamic topography. Our investigations combine the local picture provided by the perturbed-Hamiltonian formulation of xGEO astrodynamics with the global geometric dynamical portrait provided by semi-analytical, dynamical-systems theory approaches to the restricted three-body problem, harnessing these in unique ways to probe for the first time the high time-resolution details of the strongly chaotic orbital evolution of all distant cislunar space probes. Such holistic dynamical mappings of cislunar space will not only ensure that future xGEO satellites will have predictable behaviors over both the nominal (and possibly extended) mission timescales (if warranted), thus avoiding an IBEX-like situation, but that the satellites and their rocket bodies (R/B) will eventually meet their demise through atmospheric reentry (without the need to make future significant

orbital adjustments, á la ESA's INTEGRAL mission[2]). Future work will uncover the various constraints and boundaries of each theoretical and computational approach, detailed herein, thereby unraveling their inherent limitations and the precise domain in which they may be deemed valid.

6. REFERENCES

[1] A. J. Rosengren and D. J. Scheeres. Cis-lunar trajectories. In B. Cudnik, editor, *Encyclopedia of Lunar Science*, page (9 pp.). Springer, Cham, 2021.

[2] M. J. Holzinger, C. C. Chow, and P. Garretson. A Primer on Cislunar Space. Technical Report 2021-1271, AFRL, 2021.

[3] Cislunar Technology Strategy Interagency Working Group. National Cislunar Science & Technology Strategy; National Science & Technology Council, 2022. The White House Office of Science and Technology (OSTP), Washington, DC.

[4] A. J. Rosengren, D. K. Skoulidou, K. Tsiganis, and G. Voyatzis. Dynamical cartography of Earth satellite orbits. *Advances in Space Research*, 63:443–460, 2019a.

[5] J. Daquin, A. J. Rosengren, E. M. Alessi, et al. The dynamical structure of the MEO region: Long-term stability, chaos, and transport. *Celestial Mechanics and Dynamical Astronomy*, 124:335–366, 2016.

[6] T. Nie and P. Gurfil. Lunar frozen orbits revisited. *Celestial Mechanics and Dynamical Astronomy*, 130:61 (35 pp.), 2018.

[7] M. Lara. *Hamiltonian Perturbation Solutions for Spacecraft Orbit Prediction: The Method of Lie Transforms*. De Gruyter, Berlin, 2021.

[8] A. J. Schwaniger. Trajectories in the Earth-Moon Space with Symmetrical Free-Return Properties. Technical Report TN D-1833, NASA, 1963.

[9] V. A. Egorov. *Three-Dimensional Lunar Trajectories*. Israel Program for Scientific Translations, Jerusalem, 1969.

[10] W. S. Koon, M. W. Lo, J. E. Marsden, and S. D. Ross. Heteroclinic connections between periodic orbits and resonance transitions in celestial mechanics. *Chaos: An Interdisciplinary Journal of Nonlinear Science*, 10:427–469, 2000.

[11] E. J. Doedel, V. A. Romanov, R. C. Paffenroth, et al. Elemental periodic orbits associated with the libration points in the circular restricted 3-body problem. *International Journal of Bifurcation and Chaos*, 17:2625–2677, 2007.

[12] J. Casoliva, J. M. Mondelo, B. F. Villac, et al. Two classes of cycler trajectories in the Earth-Moon system. *Journal of Guidance, Control, and Dynamics*, 33:1623–1640, 2010.

[13] J. S. Parker and R. L. Anderson. *Low-Energy Lunar Trajectory Design*. Wiley, Hoboken, 2014.

[14] W. S. Koon, M. W. Lo, J. E. Marsden, and S. D. Ross. *Dynamical Systems, the Three-Body Problem and Space Mission Design*. Marsden Books, ISBN 978-0-615-24095-4, 2022.

[15] W. S. Koon, M. W. Lo, J. E. Marsden, and S. D. Ross. Low energy transfer to the Moon. *Celestial Mechanics and Dynamical Astronomy*, 81:298–314, 2001.

[16] S. D. Ross and D. J. Scheeres. Multiple gravity assists, capture, and escape in the restricted three-body problem. *SIAM Journal on Applied Dynamical Systems*, 6:576–596, 2007.

[2]Rather ironically, the rocket body (SL-12 R/B, SATCAT 27542) that placed INTEGRAL (SATCAT 27540) into its nominal distant, highly eccentric and inclined orbit on 17 October 2002 has already reentered on 30 October 2010, on account of KL-like cycles (q.v., Figure 5, *top panel*); whereas INTEGRAL will not reenter until February 2029.

[17] M. Belló, G. Gómez, and J. J. Masdemont. Invariant manifolds, Lagrangian trajectories and space mission design. In E. Perozzi and S. Ferraz-Mello, editors, *Space Manifold Dynamics: Novel Spaceways for Science and Exploration*, pages 1–96. Springer, New York, 2010.

[18] K. K. Boudad, K. C. Howell, and D. C. Davis. Dynamics of synodic resonant near rectilinear halo orbits in the bi-circular four-body problem. *Advances in Space Research*, 66:2194–2214, 2020.

[19] J. T. Fitzgerald and S. D. Ross. Geometry of transit orbits in the periodically-perturbed restricted three-body problem. *Advances in Space Research*, 70:144–156, 2022.

[20] L. T. Peterson, J. J. Rosales, and D. J. Scheeres. Osculating Keplerian elements for highly non-Keplerian orbits. *Physica D: Nonlinear Phenomena*, 455:133889 (15 pp.), 2023.

[21] B. Park and K. C. Howell. Assessment of dynamical models for transitioning from the circular restricted three-body problem to an ephemeris model with applications. *Celestial Mechanics and Dynamical Astronomy*, 32:6 (39 pp.), 2024.

[22] C. J. Scott and D. B. Spencer. Calculating transfer families to periodic distant retrograde orbits using differential correction. *Journal of Guidance, Control, and Dynamics*, 33:1592–1605, 2010.

[23] J. Ren, M. Li, and J. Zheng. Families of transfers from the Moon to distant retrograde orbits in cislunar space. *Astrophysics and Space Science*, 365:192 (21 pp.), 2020.

[24] R. Zhang, Y. Wang, H. Zhang, and C. Zhang. Transfers from distant retrograde orbits to low lunar orbits. *Celestial Mechanics and Dynamical Astronomy*, 132:41 (30 pp.), 2020.

[25] K. C. Howell and J. V. Breakwell. Almost rectilinear halo orbits. *Celestial Mechanics*, 32:29–52, 1984.

[26] K. Oshima. The use of vertical instability of l1 and l2 planar lyapunov orbits for transfers from near rectilinear halo orbits to planar distant retrograde orbits in the Earth-Moon system. *Celestial Mechanics and Dynamical Astronomy*, 131:14 (28 pp.), 2019.

[27] H. Chen, J. Liu, L. Long, et al. Lunar far side positioning enabled by a CubeSat system deployed in an Earth-Moon halo orbit. *Advances in Space Research*, 64:28–41, 2019.

[28] E. M. Zimovan-Spreen, K. C. Howell, and D. C. Davis. Near rectilinear halo orbits and nearby higher-period dynamical structures: orbital stability and resonance properties. *Celestial Mechanics and Dynamical Astronomy*, 132:28 (25 pp.), 2020.

[29] A. J. Rosengren, H. Namazyfard, and G.E.O. Giacaglia. Effects of higher-order multipoles of the lunar disturbing potential on elongated orbits in cislunar space. *European Physics Journal Special Topics*, 229:1545–1555, 2020.

[30] D. Amato, R. Malhotra, V. Sidorenko, and A. J. Rosengren. Lunar close encounters compete with the circumterrestrial Lidov–Kozai effect: The dynamical demise of Luna 3. *Celestial Mechanics and Dynamical Astronomy*, 132:35 (18 pp.), 2020.

[31] G. H. Ludwig. The orbiting geophysical observatories. *Space Science Reviews*, 2:175–218, 1963.

[32] P. Butler. Interplanetary monitoring platform. Technical Report TM-80758, NASA, 1980.

[33] A.A. Galeev, Yu. I. Gal'Perin, and L.M. Zelenyi. The INTERBALL-1 project to study solar-terrestrial physics. *Kosmicheskie Issledovaniia*, 34:339–362, 1996.

[34] F. Jansen, D. Lumb, B. Altieri, et al. XMM-Newton observatory: I. The spacecraft and operations. *Astronomy and Astrophysics*, 365:L1–L6, 2001.

[35] N. A. Eismont, A. V. Ditrikh, G. Janin, et al. Orbit design for launching INTEGRAL on the Proton/Block-DM launcher. *Astronomy and Astrophysics*, 411:L37–L41, 2003.

[36] D. J. McComas, J. P Carrico, Jr., B. Hautamaki, et al. A new class of long-term stable lunar resonance orbits: Space weather applications and the Interstellar Boundary Explorer. *Space Weather*, 9, 2011. S11002 (9 pp.).

[37] B. E. Shute and J. Chiville. The lunar-solar effect on the orbital lifetimes of artificial satellites with highly eccentric orbits. *Planetary and Space Science*, 14:361–369, 1966.

[38] D. W. Scott G. E. Cook. Lifetimes of satellites in large-eccentricity orbits. *Planetary and Space Science*, 15:1549–1556, 1967.

[39] Z. Kopal. Perturbations of the orbits of artificial satellites by an attraction of external bodies. *Icarus*, 6:298–314, 1967.

[40] M. L. Renard. Practical stability of high-eccentricity orbits quasi-normal to the ecliptic. *Journal of Spacecraft and Rockets*, 7:1208–1214, 1975.

[41] B. E. Lowrey. Ephemeris of a highly eccentric orbit: Explorer 28. *Celestial Mechanics*, 5:107–125, 1972.

[42] G. Janin and E. A. Roth. Decay of a highly eccentric satellite. *Celestial Mechanics*, 14:141–149, 1976.

[43] J.J.F. Liu, J. Segrest, and V. Szebehely. Orbit mechanics of deep space probes. *The Journal of the Astronautical Sciences*, 34:171–187, 1986.

[44] B. Érdi. Dynamics of satellites with multi-day periods. In B.A. Steves and A.E. Roy, editors, *The Dynamics of Small Bodies in the Solar System*, pages 303–307. Kluwer Academic Publishers, Dordrecht, 1999.

[45] R. Armellin, J. F. San-Juan, and M. Lara. End-of-life disposal of high elliptical orbit missions: The case of INTEGRAL. *Advances in Space Research*, 56:479–493, 2015.

[46] Y. Kozai and C. A. Whitney. Anticipated orbital perturbations of satellite 1959 Delta Two. *Smithsonian Astrophysical Observatory Special Report*, 30:15 (pp.), 1959.

[47] E. Upton, A. Bailie, and P. Musen. Lunar and solar perturbations on satellite orbits. *Science*, 130: 1710–1711, 1959.

[48] R. J. Sandifer and B. E. Shute. Effect of solar-lunar perturbations on the lifetime of Explorer XII (abstract). *The Astronomical Journal*, 67:282, 1962.

[49] V. T. Gontkovskaya and G. A. Chebotarev. Lunar and solar perturbations of Lunik III. *Soviet Astronomy*, 5:728–732, 1962.

[50] D. J. Dichmann, R. Lebois, and J. P. Carrico, Jr. Dynamics of orbits near 3:1 resonance in the Earth-Moon system. *The Journal of the Astronautical Sciences*, 60:51–86, 2014.

[51] N. S. Kardashev, B. B. Kreisman, A. V. Pogodin, et al. Orbit design for the Spektr-R spacecraft of the ground-space interferometer. *Cosmic Research*, 52:332–341, 2014.

[52] I.I. Shevchenko. *The Lidov-Kozai Effect – Applications in Exoplanet Research and Dynamical Astronomy*. Springer, Berlin, 2017.

[53] A. J. Lichtenberg and M. A. Lieberman. *Regular and Chaotic Dynamics*. Springer-Verlag, New York, 2 edition, 1992.

[54] G. Haller. *Chaos Near Resonance*. Springer-Verlag, New York, 1999.

[55] A. Celletti, C. Galeş, G. Pucacco, and A. J. Rosengren. Analytical development of the lunisolar disturbing function and the critical inclination secular resonance. *Celestial Mechanics and Dynamical Astronomy*, 127:259–283, 2017.

[56] P. Musen. On the long-period lunar and solar effects on the motion of an artificial satellite, 2. *Journal of Geophysical Research*, 66:2797–2805, 1961.

[57] M. L. Lidov. The evolution of orbits of artificial satellites of planets under the action of gravitational perturbations of external bodies. *Planetary and Space Science*, 9:719–759, 1962.

[58] R. R. Allan and G. E. Cook. The long-period motion of the plane of a distant circular orbit. *Proceedings of the Royal Society A*, 280:97–109, 1964.

[59] J. Daquin, E. Legnaro, I. Gkolias, and C. Efthymiopoulos. A deep dive into the $2g + h$ resonance: Separatrices, manifolds and phase-space structure of navigation satellites. *Celestial Mechanics and Dynamical Astronomy*, 134:6 (31 pp.), 2021.

[60] L. Blitzer. Lunar-solar perturbations of an Earth satellite. *American Journal of Physics*, 27:634–645, 1959.

[61] T. A. Ely and K. C. Howell. Dynamics of artificial satellite orbits with tesseral resonances including the effects of luni-solar perturbations. *International Journal of Dynamics and Stability of Systems*, 12: 243–269, 1997.

[62] M.L. Lidov. On the approximated analysis of the orbit evolution of artificial satellites. In M. Roy, editor, *Dynamics of Satellites*, pages 168–179. Springer-Verlag, Berlin, 1963.

[63] I. I. Shapiro. The prediction of satellite orbits. In M. Roy, editor, *Dynamics of Satellites*, pages 257–312. Academic Press, New York, 1963.

[64] A. J. Rosengren, D. J. Scheeres, and J. W. McMahon. The classical Laplace plane as a stable disposal orbit for geostationary satellites. *Advances in Space Research*, 53:1219–1228, 2014.

[65] S. Tremaine, J. Touma, and F. Namouni. Satellite dynamics on the Laplace surface. *The Astronomical Journal*, 137:3706–3717, 2009.

[66] D. G. King-Hele. The contraction of satellite orbits under the influence of air drag. III. High-eccentricity orbits ($0.2 \leqslant e < 1$). *Proceedings of the Royal Society A*, 267:541–557, 1962.

[67] A. J. Rosengren and D. J. Scheeres. Laplace plane modifications arising from solar radiation pressure. *The Astrophysical Journal*, 786:45 (13 pp.), 2014.

[68] C. D. Murray and S. F. Dermott. *Solar System Dynamics*. Cambridge University Press, Cambridge, 1999.

[69] Y. Kozai. Secular perturbations of asteroids with high inclination and eccentricity. *The Astronomical Journal*, 67:591–598, 1962.

[70] I. Takashi and K. Ohtsuka. The Lidov-Kozai oscillation and Hugo von Zeipel. *Monographs on Environment, Earth and Planets*, 7:1–113, 2019.

[71] G. D. Racca and B. H. Foing. SMART-1 mission. In B. Cudnik, editor, *Encyclopedia of Lunar Science*, page (25 pp.). Springer, Cham, 2022.

[72] T. Gallardo. Atlas of the mean motion resonances in the Solar System. *Icarus*, 184:29–38, 2006.

[73] F. Namouni and M. H. M. Morais. Resonance libration and width at arbitrary inclination. *Monthly Notices of the Royal Astronomical Society*, 493:2854—2871, 2020.

[74] A. Rawat, B. Kumar, A. J. Rosengren, and S. D. Ross. Resonance widths, chaotic zones, and transport in cislunar space. In *Proceedings of the AAS/AIAA Astrodynamics Specialist Conference*, Broomfield, Colorado, Paper AAS 24-368, 2024.

[75] F. R. Hoots, R. A. Glover, and P. W. Schumacher Jr. History of analytical orbit modeling in the U. S. Space Surveillance System. *Journal of Guidance Control and Dynamics*, 27:174–185, 2004.

[76] T. Flohrer, H. Krag, and H. Klinkrad. Assessment and categorization of TLE orbit errors for the US SSN catalogue. In *Advanced Maui Optical and Space Surveillance Technologies Conference (AMOS)*, Maui, HI, 2008.

[77] C. Früh and T. Schildknecht. Accuracy of Two-Line-Element data for geostationary and high-eccentricity orbits. *Journal of Guidance Control and Dynamics*, 35:1483–1491, 2012.

[78] C. Levit and W. Marshall. Improved orbit prediction using two-line elements. *Advances in Space Research*, 47:1107–1115, 2011.

[79] J. Sang, J. C. Bennett, and C. H. Smith. Estimation of ballistic coefficients of low altitude debris objects from historical two line elements. *Advances in Space Research*, 52:117–124, 2013.

[80] C.-C. Chao and F. Hoots. *Applied Orbit Perturbation and Maintenances.* Aerospace Press, El Segundo, CA, 2nd edition, 2018.

[81] D. Ly, R. Lucken, and D. Giolito. Correcting TLEs at epoch: Application to the GPS constellation. *Journal of Space Safety Engineering*, 61:302–306, 2020.

[82] H. Rein, D. M. Hernandez, and D. Tamayo. Hybrid symplectic integrators for planetary dynamics. *Monthly Notices of the Royal Astronomical Society*, 485:5490–5497, 2019.

[83] M. J. Holman, A. Akmal, D. Farnocchia, H. Rein, M. J. Payne, R. Weryk, D. Tamayo, and D. M. Hernandez. ASSIST: An ephemeris-quality test-particle integrator. *The Planetary Science Journal*, 4: 69 (9 pp.), 2023.

[84] H. Rein and S. F. Liu. Rebound: an open-source multi-purpose n-body code for collisional dynamics. *Astronomy and Astrophysics*, 537:A128 (10 pp.), 2015.

[85] H. Rein and D. S. Spiegel. Ias15: a fast, adaptive, high-order integrator for gravitational dynamics, accurate to machine precision over a billion orbits. *Monthly Notices of the Royal Astronomical Society*, 2:1424–1437, 2015.

[86] S. P. Hughes, R. H. Qureshi, D. S. Cooley, J. J. K. Parker, and T. G. Grubb. Verification and validation of the General Mission Analysis Tool (GMAT). In *AIAA/AAS Astrodynamics Specialist Conference*, San Diego, CA, 2014.

[87] S. P. Hughes. General Mission Analysis Tool (GMAT): GMAT application to GSFC mission design. In *International Conference on Astrodynamics Tools and Techniques (ICATT)*, Darmstadt, Germany, 2016.